INSTITUTE OF
ENERGY CONVERSION

451 Wyoming Road
Newark, DE 19716-3820
Ph: 302/831-6200
Fax: 302/831-6226
www.udel.edu/iec

UNITED STATES DEPARTMENT OF ENERGY
UNIVERSITY CENTER OF EXCELLENCE
FOR PHOTOVOLTAIC RESEARCH AND EDUCATION

August 19, 2008

Bolko von Roedern
National Renewable Energy Laboratory
1617 Cole Blvd.
Golden, CO 80401

Re: NREL Subcontract #ADJ-1-30630-12
D.5.34

This report covers research at the Institute of Energy Conversion (IEC) for the period of March 1, 2008 to March 31, 2008, under the subject subcontract. The report highlights progress and results obtained under Task 3 (Silicon solar cells).

Task 3 – Silicon Solar Cells

Passivation of silicon surface with intrinsic a-Si:H

The passivation of crystalline silicon surfaces is necessary for high performance devices as the surfaces are areas of high recombination. Amorphous silicon (a-Si) has proved to be an effective passivation layer and here at IEC we have achieved voltages above 700 mV. The level of passivation is dependent on the structure of the deposited amorphous layer. A critical factor in the growth of silicon films is the ratio of hydrogen to silane flow rate denoted here as the R ratio, where a high R ratio indicates a large about of hydrogen dilution.

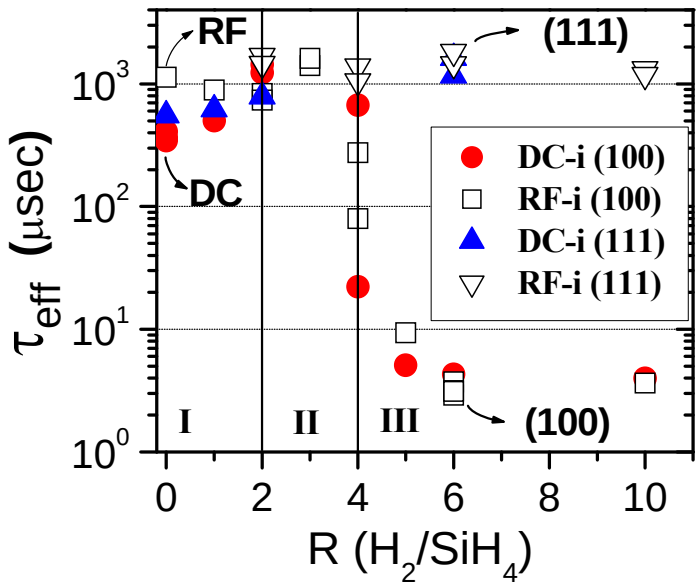

Figure 1. Effective minority carrier lifetime (τ_{eff}) on Si (100) and (111) wafers with 10 nm Si:H i-layer deposited on both sides by RF and DC plasma at variable hydrogen dilution (R).

Figure 1 shows τ_{eff} as a function of R for i-layers deposited on (100) and (111) wafers by DC and RF plasma after annealing the samples at 280°C for 10 mins. Three distinct regions can be identified in the variation of τ_{eff} with R. In region I, R < 2, τ_{eff} depends on the plasma process; namely, DC plasma deposited i-layers at R = 0 show slightly lower lifetime, ~ 500 µsec, than RF plasma deposited i-layers, > 1 msec, irrespective of the wafer surface orientation. τ_{eff}, however, becomes similar for RF and DC plasma deposited i-layers at R > 2, region II and III, implying little or no adverse effect of ion damage in the DC process on Si surface passivation. In region III, R > 4, the measured τ_{eff} exhibits a pronounced Si surface orientation dependence. The values of τ_{eff} sharply decrease to < 10 µsec on (100) wafers, while on (111) wafers they remain > 1 msec even at R = 10. In the following section, the DC i-layers are further examined using cross-sectional transmission electron microscopy (XTEM).

XTEM images of c-Si / a-Si:H interfaces

Figure 2 shows the deposition of a layer of silicon deposited by PECVD on polished crystalline silicon substrates. In image (a), the silicon layer shows a high degree of crystallinity with epitaxial growth so that there is not a clear interface between the substrate and the deposited silicon layer. The lifetime for this sample is low so that the surface is essentially unpassivated as shown in Figure 1 where the R6 lifetime on (100) is only 40 µs.

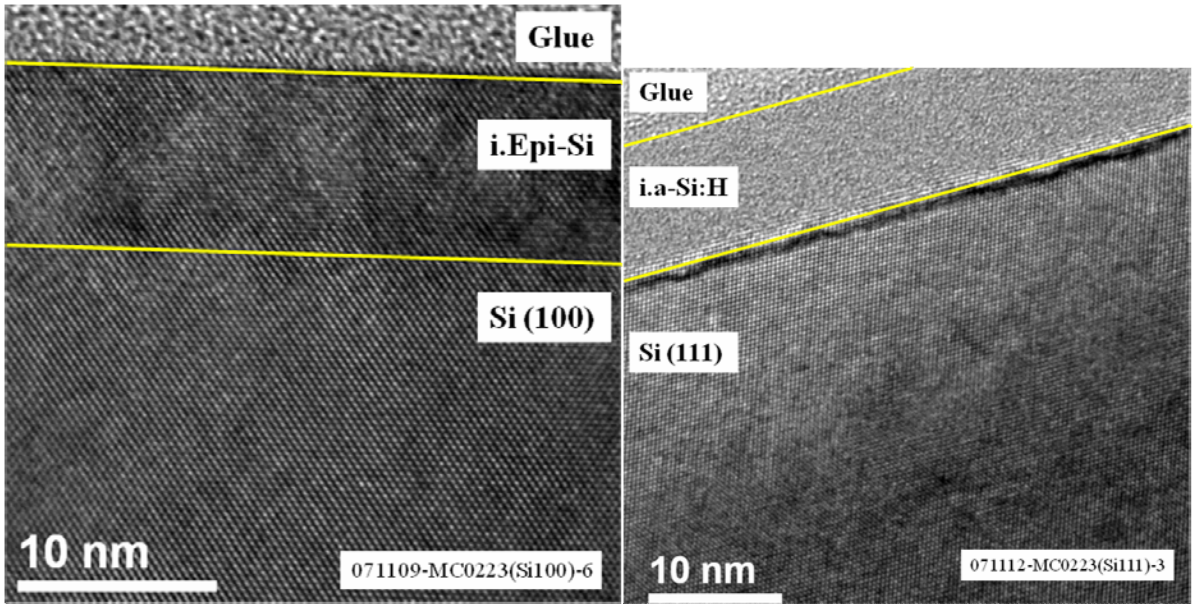

(a) (b)

Figure 2. TEM of R6 DC i-layer deposited on silicon substrates. (a) with a (100) orientation and (b) with a (111) orientation.

In contrast, the image of (b) shows a completely amorphous layer on top of the crystalline silicon substrate and the lifetime is well above 1 ms. The only difference between the two images is the substrate orientation. The (111) orientation has suppressed crystallinity leading to an amorphous film.

To understand the wafer orientation dependence of τ_{eff}, i-layer structure and optical properties are determined from VASE measurements on the same samples used for lifetime testing. Figure 3 shows the imaginary part of the pseudo dielectric constant, ε_2, as a function of photon energy (E) for i-layers deposited on (100) and (111) wafers at R = 6. A broad featureless spectrum for the R = 6 i-layer on Si (111) wafer is indicative of amorphous Si:H structure. However, the same Si:H layer deposited on (100) wafer exhibits the identical optical constants as crystalline silicon, which implies that the film is epitaxial; this is confirmed by transmission electron microscopy (TEM). This indicates that any epitaxial growth of i-layers severely deteriorates the surface passivation quality of the deposited layer and τ_{eff} drops to less than 10 μsec (see Figure 1).

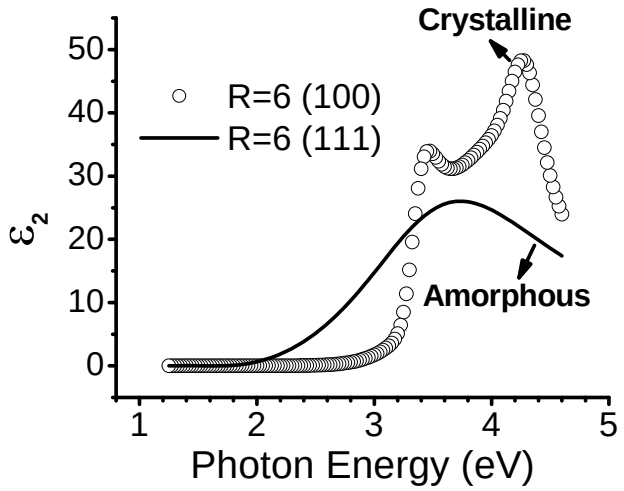

Figure 3. Imaginary part of pseudo-dielectric function (ε_2) as a function of photon energy (E) for the Si:H i-layers deposited with R = 6 on (100) and on (111) wafers.

Figure 4 shows the deposition of two layers as would be typical in a solar cell structure. An R6 i-layer followed by a p-type deposition passivates and forms a junction. In both cases the films are completely amorphous and we see no crystallinity forming with the thicker film. The other feature to note is that there is no interface layer between the i-layer and the crystalline silicon substrate as is evident in the previous image. The loss of interface layer is believed to be due to the further annealing that this layer has experienced over that of Figure 2(b).

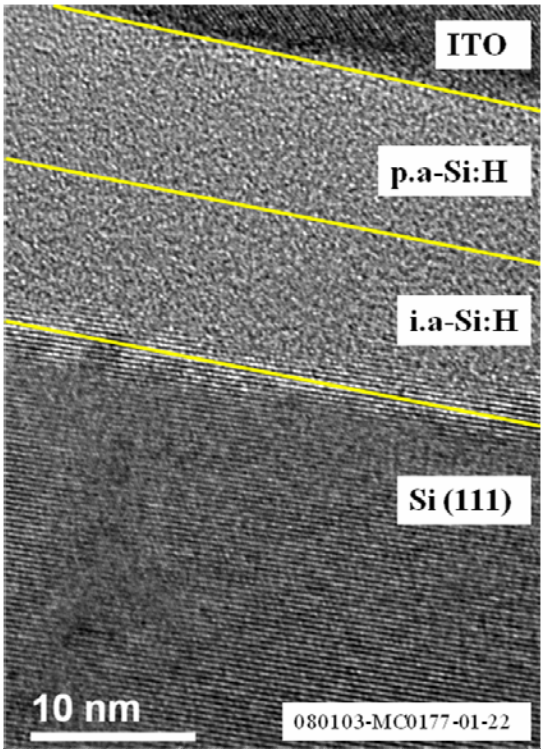

Figure 4. R6 DC i-layer and p-layer on (111) Si substrate.

The XTEM final image is for a deposition on (111) material where there is a very high dilution of the growth with hydrogen and R = 40. In this case we get the growth of a microcrystalline film on the substrate. The crystal structure of the film is very poor unlike that of Figure 2(a) where epitaxial growth was seen. The loss of amorphous film has caused a loss of passivation in this layer and the lifetime has dropped to under 100 µs.

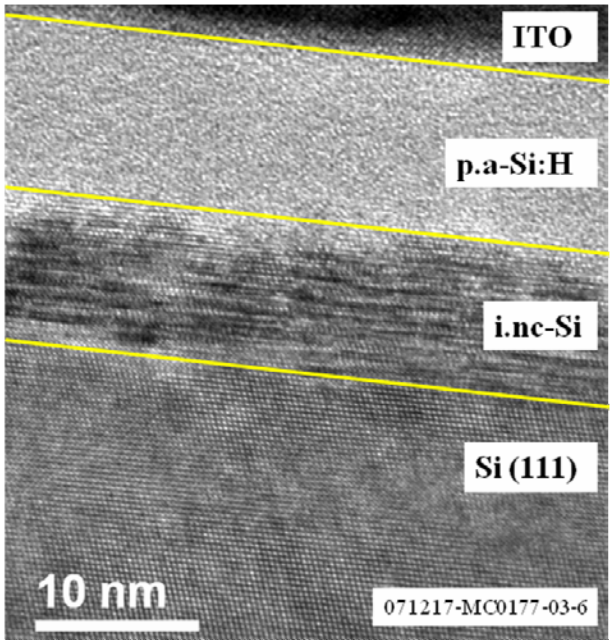

Figure 5. R40 DC i-layer and p-layer on (111) Si substrate.

The XTEM images show that good passivation and low surface recombination is only achieved with an amorphous film. Amorphous films grow more readily on (111) surfaces and by using layers with a lower hydrogen dilution.

Fabrication of Back Junction Devices

Figure 6(a) shows the schematic structure of the front silicon heterojunction (SHJ) and interdigitated back contact-silicon heterojunction (IBC-SHJ) cells. All the a-Si:H layers are deposited using identical plasma conditions in both cell structures. The i-layers are deposited with R = 2 to suppress the growth of microcrystalline silicon. The illuminated J-V curves are compared in Figure 6(b). The V_{OC} values (~690 mV) are the same in both structures, while J_{SC} is higher (~ 3 mA/cm^2) in the IBC structure due to reduced optical loss at the front illuminating side. However, the FF in this IBC structure is very low due to the "S" shape J-V curve. This result indicates the necessity of further optimization of IBC-SHJ solar cells. There are two major functional differences between the front-junction and IBC device structures:
(i) the carrier transport is one dimensional in front-junction SHJ cell, while the IBC-SHJ structure has a two dimensional transport mechanism, and (ii) the front i-layer in front-junction SHJ cell gets illuminated and generates photo carriers, while the i-layer in the IBC structure is in the dark and does not generate carriers.

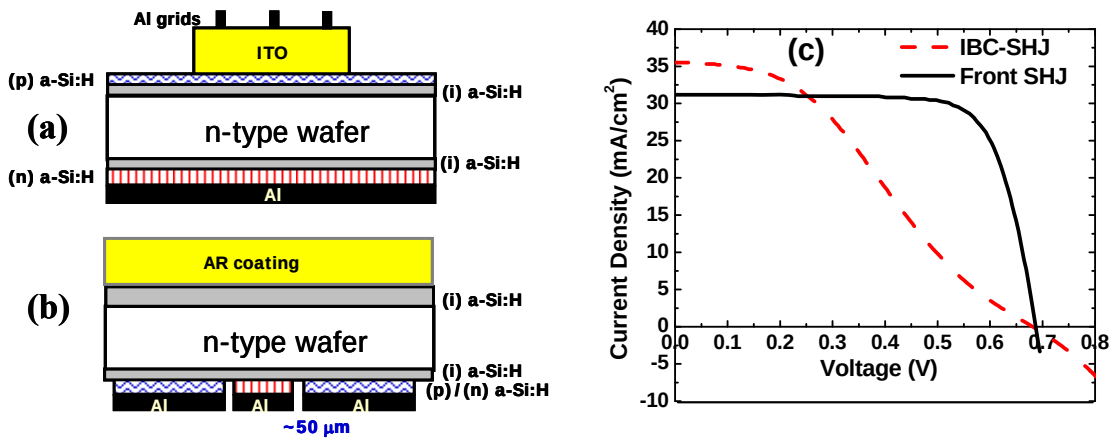

Figure 6. Schematic structures of (a) front junction SHJ cell, (b) IBC-SHJ cell, and (c) comparison of the illuminated J-V curves in two cell structures.

2D numerical simulation of IBC-SHJ solar cell

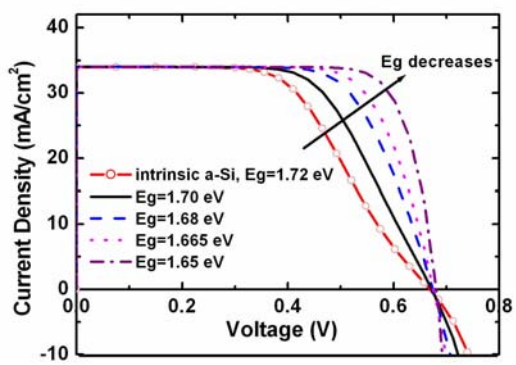

Figure 7. Simulated J-V curves for IBC-SHJ cells [structure shown in Figure 8 (b)] under illumination with variable band gap of the intrinsic a-Si buffer layer.

We have performed 2D numerical simulation using a "Sentaurus Device" simulator (called DESSIS in its old version). Both the experimental results and numerical simulation confirm that low FF with an "S" shape J-V appears in IBC-SHJ structure due to the presence of an intrinsic a-Si:H buffer layer only in the p-type emitter strip. This suggests the existence of a hole transport barrier across the intrinsic a-Si:H buffer layer.

The low FF and "S" shape J-V can arise from the hole transport barrier due to the enhanced valence band offset generated by the intrinsic buffer layer. Hence the effect of band gap of the intrinsic a-Si buffer layer on IBC-SHJ cell performance is studied. Again, the surface passivation effects of the different buffer layers are assumed to be the same, while electron affinities of the buffer layers are assumed constant. Figure 7 shows the illuminated J-V

characteristics obtained from simulation for intrinsic a-Si buffers as a function of band gaps. A substantial effect of the band gap is evident on FF, which increases from 55% to >78% as the band gap of the buffer layer is reduced by 0.07 eV.

To simultaneously maintain high V_{OC} and J_{SC} with narrower band gap buffer layers, high passivation quality of the buffer layer is also required. Intrinsic a-Si:H buffer layers with narrower band gaps are developed by varying plasma process parameters without alloying with other semiconductors like Ge. Figure 8(a) shows the Tauc's plot for two different a-Si:H layers, where the dashed (black) curve represents the control buffer layer, and the solid (red) curve indicates the newly developed i-layer. It can be seen that the band gap of the new i-layer is ~0.04 eV narrower than that of the control layer. The τ_{eff} values shown beside the curves indicate that they have similar passivation quality. Figure 8(b) compares the illuminated J-V curves for the IBC-SHJ cells with 5 nm narrower band gap i-layer and 10 nm higher band gap i-layer. An IBC-SHJ cell with efficiency of 13.5% and FF of 77% is achieved with the narrower band gap i-layer. However, the V_{OC} and J_{SC} is lower than the standard i-layer, which is due to insufficient surface passivation in the gap between the p- and n- strips.

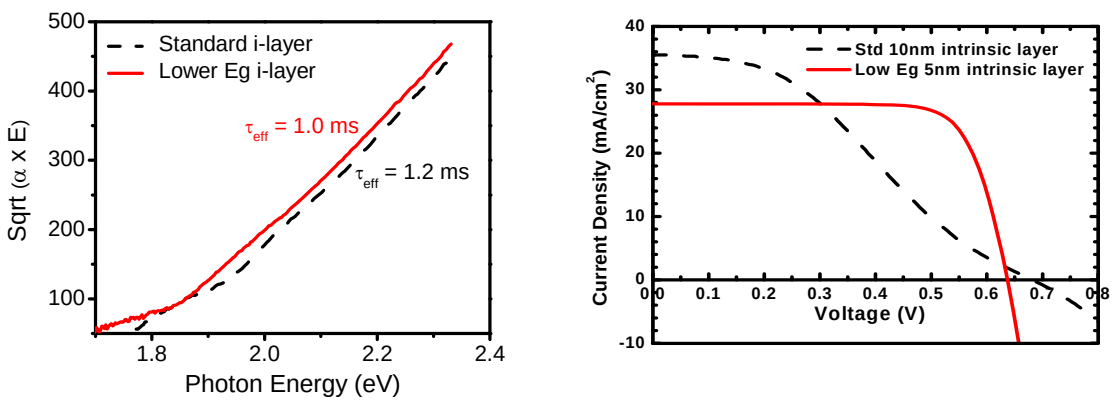

(a) (b)

Figure 8. (a) Tauc's plot for control (black dashed curve) and newly developed (red solid curve) intrinsic a-Si:H layers, and (b) illuminated J-V curves of IBC-SHJ cells with a 5 nm lower band gap i-layer and 10 nm standard i-layer.

Best regards,

Robert W. Birkmire
Director